

Near ultraviolet photolysis of ammonia and methylamine studied by H Rydberg atom photofragment translational spectroscopy

BY M. N. R. ASHFOLD, R. N. DIXON, M. KONO, D. H. MORDAUNT†
AND C. L. REED

School of Chemistry, University of Bristol, Bristol BS8 1TS, UK

H(D) Rydberg atom photofragment translational spectroscopy has been used to provide new insights into the primary photochemistry of methylamine, ammonia and various of their respective isotopomers following excitation at wavelengths in the near ultraviolet (UV). The bimodal appearance of the total kinetic energy release (TKER) spectra associated with H atom production in the near UV photolysis of methylamine is consistent with there being both ‘dynamical’ (high TKER) and ‘statistical’ (slower) contributions to the total H + CH₃NH dissociation yield. Both contributions arise as a result of one H atom tunnelling through (or passing over) an earlier barrier in the N–H dissociation coordinate of the \tilde{A} state potential energy surface and then evolving into the region of the conical intersection connecting the \tilde{A} state and ground-state surfaces. ‘Dynamical’ energy disposal is associated with those molecules which pass directly through this conical intersection *en route* to the ground-state (H + CH₃NH(\tilde{X})) asymptote, whilst the ‘statistical’ contribution is attributed to those molecules that ‘miss’ the conical intersection on the first traversal and only make the $\tilde{A} \rightarrow \tilde{X}$ transfer on a later encounter. This interpretation has inspired further consideration of the form of the TKER spectra derived from TOF measurements of the H/D atom products arising in the dissociation of various isotopomers of ammonia following excitation to the 0⁰ and 2¹ levels of their respective \tilde{A} states. A similar model which associates ‘dynamical’ energy disposal with those molecules that pass through the \tilde{A}/\tilde{X} conical intersection during bond extension, and ‘statistical’ kinetic energy release with those that transfer during N–H(D) bond compression, appears to provide a qualitative explanation for the way the observed H and/or D atom yields and their associated TKER spectra vary with excitation wavelength (0⁰ versus 2₀¹ band excitation) and isotopic composition.

1. Introduction

Photodissociation plays a key role in cycling gas phase molecules in the atmospheres of Earth and of the various planets. Recent laboratory studies of the photochemistry of, for example, ozone (Miller *et al.* 1994; Ball *et al.* 1995; Takahashi *et al.* 1996) and methane (Mordaunt *et al.* 1993) are providing new insights into the chemistry prevailing within our own stratosphere (Mack *et al.* 1996) and in the atmospheres of

† Present address: Department of Chemistry, University of California Berkeley, CA 94720, USA.

various of the moons of Jupiter and Saturn, e.g. Titan (Lara *et al.* 1994), respectively. Here we present the results of experimental studies of the primary photochemistry of ammonia (NH_3) and methylamine (CH_3NH_2) following photoexcitation to their respective first excited singlet electronic states. The observable in these experiments is a high resolution time-of-flight (TOF) spectrum of the atomic hydrogen photoproducts; the technique relies on the remarkable stability of the high- n Rydberg states of atomic H and D.

The first ($\tilde{A}^1A_2'' - \tilde{X}^1A_1'$) absorption band of ammonia spans the wavelength range 170–220 nm and is associated with promotion of one of the nitrogen lone pair electrons to an excited orbital with mixed Rydberg (3s)–antibonding valence (σ^*) character (Douglas 1963; Runau *et al.* 1977; Vaida *et al.* 1984; McCarthy *et al.* 1987; Rosmus *et al.* 1987; Ashfold *et al.* 1996). The absorption spectrum exhibits a clear progression in ν_2' , the excited state out-of-plane (umbrella) bending mode, reflecting the planar \leftarrow pyramidal change in minimum energy configuration upon electronic excitation. The corresponding $\tilde{A}-\tilde{X}$ absorption system in methylamine (190 nm $< \lambda <$ 240 nm) also exhibits regular but diffuse vibronic structure which has been assigned (Tsuboi *et al.* 1969) to progressions involving the NH_2 wagging (ν_9) and CH_3 rocking (ν_{14}) modes. However, a more recent analysis (Taylor *et al.* 1995) of resonance enhanced multiphoton ionization (REMPI) spectra of jet-cooled samples of the four isotopomers CH_3NH_2 , CH_3ND_2 , CD_3NH_2 and CD_3ND_2 suggests that the second Franck–Condon active mode is actually the ν_4 (NH_2 scissors) vibration. Such an interpretation is appealing in that it implies that electronic excitation induces a trend towards sp^2 hybridization at the N centre analogous to that in ammonia.

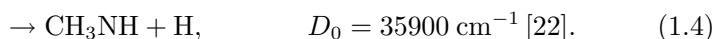
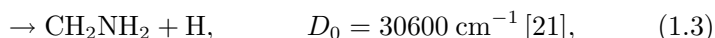
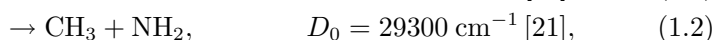
The dissociation dynamics of NH_3 molecules following photoexcitation to their \tilde{A}^1A_2'' excited state have been much studied, with the result that this system is often cited as a textbook example of a molecular photofragmentation process (Ashfold *et al.* 1996). Linewidth studies show that the excited state lifetime varies sensitively with H/D isotopic substitution and with the ν_2 quantum number; in all isotopomers, the level with $\nu_2 = 1$ is the most long lived. Such behaviour has been rationalized in terms of vibrational predissociation on the \tilde{A} state potential energy surface. Ammonia molecules in their \tilde{A} state are quasi-bound; dissociation from the two lowest vibrational levels (i.e. those with $\nu_2 \leq 1$) occurs predominantly, if not exclusively, via H atom tunnelling through a barrier in the exit channel leading to the products $\text{H} + \text{NH}_2$. This barrier arises as a natural consequence of the Rydberg (3s) \rightarrow antibonding valence (σ^*) orbital evolution as one N–H bond is extended (Runau *et al.* 1977; Rosmus *et al.* 1987); the barrier height is least (and tunnelling consequently most facile) at planar geometries (Ashfold *et al.* 1985; McCarthy *et al.* 1987; Rosmus *et al.* 1987). \tilde{A} state ammonia molecules with $\nu_2' > 1$, or with excitation in vibrational modes other than ν_2 , have sufficient internal energy that, if redistributed appropriately, dissociation can occur by passage over (rather than through) the exit channel barrier on the \tilde{A} state surface.

Planarity, or otherwise, also influences the asymptotic product correlations. For planar configurations, the \tilde{X} state of ammonia correlates with the excited products $\text{H} + \text{NH}_2(\tilde{A}^2A_1)$, whilst the parent \tilde{A} state correlates with the ground-state products $\text{H} + \text{NH}_2(\tilde{X}^2B_1)$. Away from planarity, the \tilde{X} and \tilde{A} states of ammonia have the same (A') electronic symmetry. Thus these two potential energy surfaces can only ‘cross’ at planar geometries and, consequently, there is a conical intersection (CI) between the \tilde{A} and \tilde{X} state surfaces, at planar geometries, in the H– NH_2 exit channel. As a result, the parent \tilde{A} state surface shows a deep well in this exit channel, which acts

as a funnel, accelerating many of the dissociating trajectories through this narrow region of configuration space onto the \tilde{X} state surface and thence to the ground-state products. Energetic considerations dictate that ammonia photolysis at $\lambda \geq 206$ nm can only lead to ground-state products; the excited $\text{H} + \text{NH}_2(\tilde{A})$ products become increasingly important at shorter photolysis wavelengths, accounting for *ca.* 30% of the total dissociation yield at 193 nm (Biesner *et al.* 1989).

Previous H atom photofragment translational spectroscopy (PTS) experiments involving the ammonia molecule have highlighted the profound influence of this CI on the quantum state population distributions within the resulting $\text{NH}_2(\tilde{X})$ fragments. A substantial fraction of these products are formed with little vibrational excitation, but with considerable rotational excitation, specifically distributed in the form of *a*-axis rotation (Biesner *et al.* 1988, 1989; Ashfold *et al.* 1990; Dixon 1996; Mordaunt *et al.* 1996*a, b*). This very non-statistical energy disposal is a natural consequence of the CI amplifying any out-of-plane bending motion in the parent NH_3 molecule into *a*-axis rotation of the fragment. The later studies also identify an unresolved, 'statistical' contribution to the total $\text{H} + \text{NH}_2(\tilde{X})$ product yield, the relative importance of which depends sensitively upon H/D isotopic substitution and the parent vibrational level. This has been attributed to, and modelled in terms of, $\tilde{A} \rightarrow \tilde{X}$ internal conversion (IC), followed by unimolecular decay (Mordaunt *et al.* 1996*b*), but the mechanism of the IC process remains an open question.

Methylamine photodissociation has received much less attention but inevitably, given the greater number of degrees of freedom, it has a potentially richer photochemistry. Thermochemical considerations suggest the possibility of seven different fragmentation channels following absorption of a 220 nm photon (the wavelength corresponding to the peak of the first absorption band) (Hwang *et al.* 1990; Reed *et al.* 1996). Classical photochemical experiments (Michael *et al.* 1963), together with more recent PTS studies (Waschewsky *et al.* 1995; Reed *et al.* 1996), suggest that channels (1.1)–(1.4) all contribute to the primary UV photochemistry of methylamine, with channel (1.4) contributing more than 75% of the total dissociation yield:



Interpreting this finding, and the deduced form of the energy partitioning in the various dissociation products, relies heavily on the theoretical work of Kassab *et al.* (1983) and Dunn & Morokuma (1996). The latter workers present cuts through *ab initio* potential energy surfaces for the \tilde{A} and \tilde{X} states of methylamine. These show that the \tilde{A} state potential for both C–N and N–H bond fission (channels (1.2) and (1.4), respectively) is, in each case, characterized by a small barrier at short range and, at larger bond extensions, by a conical intersection with the \tilde{X} state surface at geometries for which the NH_2 moiety and one C–H bond are coplanar. Thus the topology of the \tilde{A} and \tilde{X} state surfaces of methylamine, along the N–H dissociation coordinate, is qualitatively similar to that in ammonia. Dunn & Morokuma (1996) also calculate that: (i) the barrier to C–N bond fission on the \tilde{A} state surface is somewhat larger than that for N–H bond rupture (consistent with the observed dominance of channel (1.4) following near UV excitation of CH_3NH_2); and (ii) C–H bond extension in the \tilde{A} state correlates adiabatically with the excited products

$\text{H} + \text{CH}_2\text{NH}_2(\tilde{A})$ —a process which is endoergic for all $\lambda \gtrsim 190$ nm. Thus any experimentally observed products attributable to dissociation channel (1.3) must arise as a result of IC from the initially populated \tilde{A} state and subsequent dissociation on the ground-state surface. Such is broadly consistent with experimental findings (Waschewsky *et al.* 1995): the total kinetic energy release (TKER) spectra associated with the $\text{H} + \text{CH}_3\text{NH}$ and $\text{CH}_3 + \text{NH}_2$ product channels both peak away from zero kinetic energy, consistent with dissociation on a surface for which there is a barrier to the reverse reaction, whilst the TKER spectrum attributed to the $\text{H} + \text{CH}_2\text{NH}_2$ channel is deduced to peak near zero. Recent work from our own group (Reed *et al.* 1996), however, indicates that these ‘slow’ H atoms actually also arise via dissociation channel (1.4).

Here we consider high-resolution TKER spectra of the H(D) atom photofragments arising in the photodissociation of various of the H/D isotopomers of ammonia and methylamine following monochromatic excitation in the near UV. Much of the ammonia data has been presented previously (Mordaunt *et al.* 1996*a, b*); the observations and much of the interpretation that derives therefrom will only be summarized briefly. The TKER spectra of the H(D) atoms resulting from methylamine photolysis appear bimodal, suggesting contributions both from direct bond fission and from a slower, more ‘statistical’ unimolecular decay process. The deduced importance of dissociation channel (1.4) as the source of the ‘slow’ H(D) atoms, arising via unimolecular decay after IC from the initially populated \tilde{A} state of methylamine, is most readily accommodated by assuming that IC occurs in the region of the \tilde{A}/\tilde{X} conical intersection in the N–H exit channel. Given this conclusion, we consider the evidence for and against such an explanation for the ‘statistical’ component of the H(D) atom TKER spectrum arising in the UV photolysis of ammonia.

2. Experimental

The apparatus used to measure H-atom photofragment translational spectra and the ‘tagging’ of the H atoms has been described previously (Morley *et al.* 1992, 1993; Mordaunt *et al.* 1996*a, b*; Reed *et al.* 1996). A pulsed skimmed supersonic molecular beam of the chosen parent molecule (seeded in Ar) is crossed, orthogonally, by the output of three dye lasers. Laser 1, the output of which is frequency doubled and then mixed to produce light in the range $200 < \lambda < 240$ nm, induces photolysis. The resulting H(D) atom photofragments are then ‘tagged’ via a two-colour two-photon (121.6 and 365.7 nm) excitation to a high- n Rydberg state. The detected H(D) atoms fly a known field-free distance along the third orthogonal axis and are field-ionized immediately before detection. The detector output is amplified and sent to a digital storage oscilloscope for display. This transient TOF spectrum is transferred to a computer via a GPIB interface and allowed to accumulate for (typically) 10^4 laser shots. Energy and momentum conservation allows conversion of the accumulated TOF spectra to TKER spectra as described in the publications cited above.

3. Results and discussion

(a) Ammonia photolysis: the ‘dynamical’ channel

The observable in all of these experiments is the H atom yield arriving at a detector located a known distance, d , from the photolysis volume, recorded as a function of

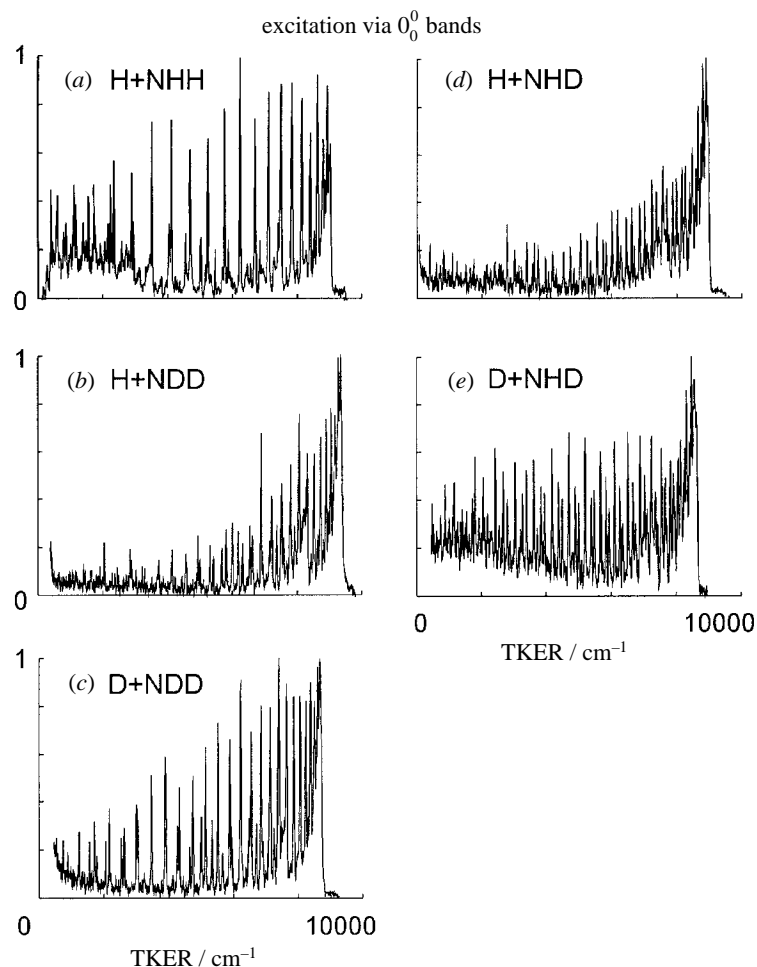


Figure 1. TKER spectra (all normalized to the same peak intensity and all plotted on a common energy scale) for the fragments resulting from photolysis of jet-cooled samples of the various isotopomers of ammonia: (a) $\text{NH}_3 \rightarrow \text{H} + \text{NH}_2$ excited at $46\,200\text{ cm}^{-1}$; (b) $\text{NHD}_2 \rightarrow \text{H} + \text{ND}_2$ at $46\,529\text{ cm}^{-1}$; (c) $\text{ND}_3 \rightarrow \text{D} + \text{ND}_2$ at $46\,708\text{ cm}^{-1}$; (d) $\text{NH}_2\text{D} \rightarrow \text{H} + \text{NHD}$ at $46\,359\text{ cm}^{-1}$; and (e) $\text{NHD}_2 \rightarrow \text{D} + \text{NHD}$ at $46\,529\text{ cm}^{-1}$, i.e. at the peaks of their respective $\tilde{A}-\tilde{X}$ origin absorptions, with, in each case, ε aligned perpendicular to the TOF axis.

time after the photolysis laser pulse. Signal arriving with a particular TOF, t_{H} , can be related to the corresponding photofragment TKER, $E_{\text{kin,total}}$, via the relationship

$$E_{\text{kin,total}} = E_{\text{kin,H}} + E_{\text{kin,R}} = \frac{1}{2}m_{\text{H}} \left(1 + \frac{m_{\text{H}}}{m_{\text{R}}} \right) \left(\frac{d}{t_{\text{H}}} \right)^2, \quad (3.1)$$

where R is the fragment partnering the detected H atom (e.g. NH_2 in the case of NH_3 photolysis, or a fragment having chemical formula CH_4N in the case of methylamine photodissociation). Clearly, an equivalent expression holds when detecting D atom fragments arriving with a TOF t_{D} .

Figures 1 and 2 show representative TKER spectra obtained by monitoring H and/or D atoms resulting from photolysis of jet cooled samples of the various isotopomers of ammonia following excitation within their respective $\tilde{A}-\tilde{X}0_0^0$ and 2_0^1

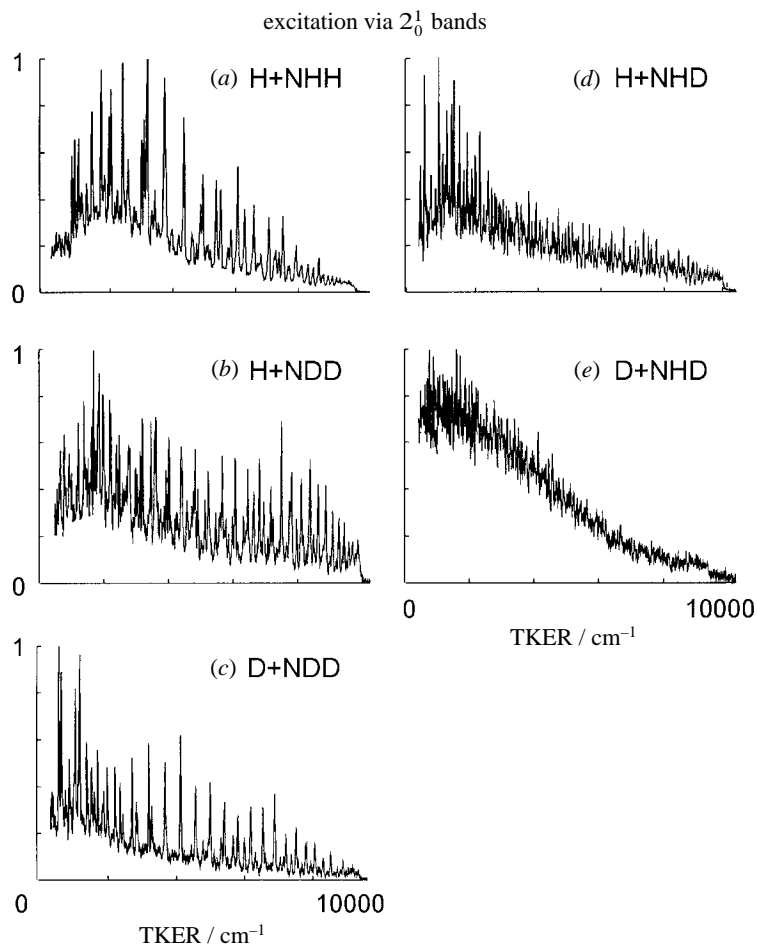


Figure 2. TKER spectra (all normalized to the same peak intensity and all plotted on a common energy scale) for the fragments resulting from photolysis of jet-cooled samples of the various isotopomers of ammonia: (a) $\text{NH}_3 \rightarrow \text{H} + \text{NH}_2$ excited at $47\,069\text{ cm}^{-1}$; (b) $\text{NHD}_2 \rightarrow \text{H} + \text{ND}_2$ at $47\,264\text{ cm}^{-1}$; (c) $\text{ND}_3 \rightarrow \text{D} + \text{ND}_2$ at $47\,362\text{ cm}^{-1}$; (d) $\text{NH}_2\text{D} \rightarrow \text{H} + \text{NHD}$ at $47\,155\text{ cm}^{-1}$; and (e) $\text{NHD}_2 \rightarrow \text{D} + \text{NHD}$ at $47\,264\text{ cm}^{-1}$, i.e. at the peaks of their respective $\tilde{A}-\tilde{X} 2_0^1$ absorptions, with, in each case, ε aligned perpendicular to the TOF axis.

bands. The sharp structure evident in these spectra is assignable in terms of formation of $\text{NH}_2/\text{NHD}/\text{ND}_2$ fragments carrying little vibrational excitation, but with a wide spread of rotational energies; in all cases, however, this rotational energy is concentrated in the form of a -axis rotation of the fragment (Biesner *et al.* 1988, 1989; Ashfold *et al.* 1990; Dixon 1996; Mordaunt *et al.* 1996*a, b*). Similar sharp structure was observed in previous (lower resolution) H atom PTS studies of NH_3 photolysis at still shorter wavelengths, $\lambda \geq 193\text{ nm}$, i.e. for photoexcitation of \tilde{A} state vibronic levels with $v_2' \leq 6$ (Biesner *et al.* 1988). These spectra derive from TOF measurements made with the ε vector of the photolysis laser radiation aligned perpendicular to the TOF axis. Each photolysis has been investigated as a function of θ , the angle between ε and the H(D) atom recoil velocity vector, \mathbf{v} . Such studies (Mordaunt *et al.* 1996*a*) reveal that, although the angular dependence of the *total* H(D) atom flux is rather isotropic, ε and \mathbf{v} are nonetheless strongly correlated, but in a manner that varies

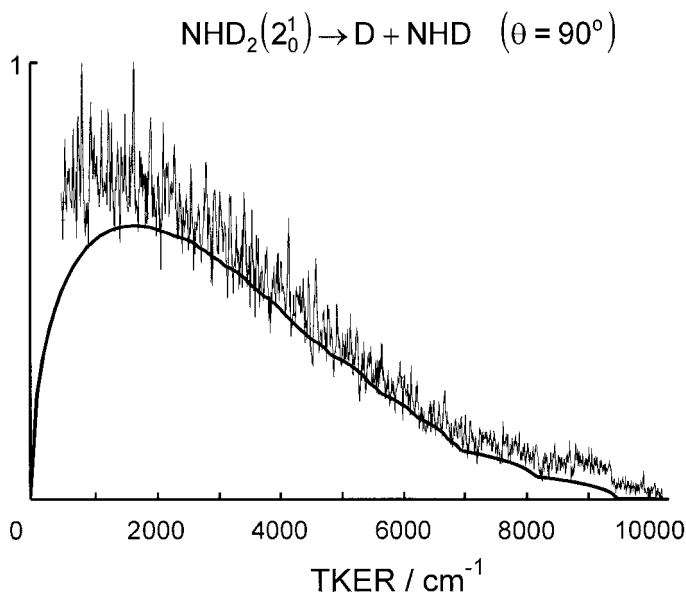


Figure 3. Expanded view of the TKER spectrum of the D + NHD fragments resulting from photodissociation of NHD_2 at 47264 cm^{-1} . The solid curve shows the TKER spectrum expected for a wholly 'statistical' energy partitioning such as might occur for dissociation of highly vibrationally excited $\text{NHD}_2(\tilde{X})$ molecules formed by IC from the initially photoexcited \tilde{A} state.

with the particular v, N rovibrational state in which the partner $\text{NH}_2/\text{NHD}/\text{ND}_2$ fragment is formed. H(D) atoms formed in association with rotationally 'cold' fragments show with greatest probability when $\theta = 90^\circ$ (i.e. as in figures 1 and 2), whilst those fragments carrying the highest levels of a -axis rotational excitation show most clearly when ϵ is parallel to the TOF axis (i.e. when $\theta = 0^\circ$).

The following explanation for such observations is phrased specifically in terms of NH_3 photodissociation, but analogous arguments hold for the lower symmetry mixed isotopomers also. \tilde{A} state ammonia molecules have a planar equilibrium geometry and the $\tilde{A}-\tilde{X}$ transition moment, μ_{parent} , lies perpendicular to this plane. Following excitation to the 0^0 and 2^1 levels, the dissociating molecules tunnel through the exit channel barrier and emerge with a range of out-of-plane configurations (centred about planarity) and momenta. Those that approach the CI with (essentially) planar geometries pass straight through to the ground-state surface. There are no torques acting to generate out-of-plane motion and the H and $\text{NH}_2(\tilde{X})$ fragments separate in the plane perpendicular to μ_{parent} and thus to ϵ , i.e. the $\text{NH}_2(\tilde{X})$ fragments have little internal excitation and the partner H atoms (which, by energy conservation, appear in the early part of the TOF spectrum) show predominantly at $\theta = 90^\circ$. Expressed in terms of the classical anisotropy parameter, β , these fragments show an angular distribution with $\beta \sim -1$, characteristic of dissociation following a 'perpendicular' photoexcitation process. At the other extreme, molecules that approach the CI with markedly non-planar geometries have to be drawn into the deep well associated with the CI in order to acquire the necessary planar (or near planar) geometry required for $\tilde{A} \rightarrow \tilde{X}$ surface crossing and dissociation. Inevitably, this provides the nuclei with an out-of-plane acceleration and also tends to amplify any existing out-of-plane nuclear motion. This angular momentum carries over into the asymptotic products in the form of a -axis rotation in the $\text{NH}_2(\tilde{X})$ fragments and counterbalancing orbital

angular momentum of the H atom about the NH₂ moiety. Hence the observation that the (slow) H atoms that partner the most highly rotationally excited NH₂(\tilde{X}) fragments are thrown out of the original plane of the excited state molecule and, in fact, appear with greatest probability at $\theta \sim 0^\circ$, implying a positive β —a result that, at first sight, might suggest that the fragments arise as a result of a ‘parallel’ photoexcitation process!

The TKER spectra shown in figures 1 and 2 also exhibit an underlying continuum, which generally becomes more pronounced at low recoil energies, is more evident in the case of dissociation from the 2¹ level than from the 0⁰ level of the \tilde{A} state, and is most evident in those dissociations which yield the asymmetric NHD fragment. As figure 3 shows, the shape of the most dramatic of these underlying contributions, that observed for the fragmentation NHD₂ → D + NHD, is well described by a statistical distribution based on a harmonic oscillator plus rigid rotor density of states for the three vibrational and three rotational degrees of freedom of the NHD product, and a factor of $(E_{\text{kin}})^{1/2}$ for the relative translational motion of the recoiling fragments. Such a ‘statistical’ energy disposal has been attributed to the unimolecular decay of highly vibrationally excited ground-state molecules formed following IC from the initially populated \tilde{A} state. Before addressing further the mechanism of this $\tilde{A} \rightarrow \tilde{X}$ internal conversion process in ammonia, we first consider the fragmentation of \tilde{A} state methylamine molecules, to see if it can offer additional insights.

(b) UV photolysis of methylamine

Figure 4 shows TKER spectra of the H + CH₄N fragments resulting from CH₃NH₂ photolysis at three arbitrarily chosen, quite widely separated, near UV wavelengths: 233.3, 225.4 and 219.0 nm. The spectra recorded at the longer excitation wavelengths show some resolved vibrational structure. Each is characterized by a rising ‘tail’ at low TKER—indicative of some branching into fragments with high internal energy. Studies of the relative H/D atom yields resulting from UV photolysis of each of the isotopomers CH₃NH₂, CD₃NH₂, CH₃ND₂ and CD₃ND₂, the form of the respective H/D TOF spectra and their invariance to laser pulse energy indicate that most, if not all, of the observed H(D) atoms arise as a result of N–H (N–D) bond fission (Reed *et al.* 1996)—consistent with the earlier estimates of the relative importances of fragmentation channels (1.3) and (1.4) (Michael *et al.* 1963). The maximum fragment TKER observed in each case, indicated by the vertical arrows in figure 4, implies $D_0(\text{H–NHCH}_3) = 34\,550 \pm 200 \text{ cm}^{-1}$ (Reed *et al.* 1996).

The overall shape of these TKER spectra accords with that deduced in another PTS study of the products arising in the 222 nm photolysis of CH₃NH₂ and some of its isotopomers (Waschewsky *et al.* 1995). The total CH₄N fragment yield was shown to be isotropic (within the experimental uncertainty). This PTS study involved mass spectrometric product detection and so was also able to investigate gross features of the energy disposal associated with fragmentation channels (1.1) and (1.2). The TKER spectra of the H₂ elimination products from channel (1.1) and of the products arising from the C–N bond fission (1.2) were both found to peak at TKER $\gg 0$, consistent with the presence of activation barriers in the reaction coordinates for the corresponding back reactions (Waschewsky *et al.* 1995).

The present work is only sensitive to dissociations yielding H/D atoms (i.e. channels (1.3) and (1.4)) and from hereon we focus attention on these two possible primary processes. *Ab initio* calculations (Dunn *et al.* 1996) show that \tilde{A} state methylamine molecules correlate with the excited products H + CH₂NH₂(\tilde{A})—a process that is

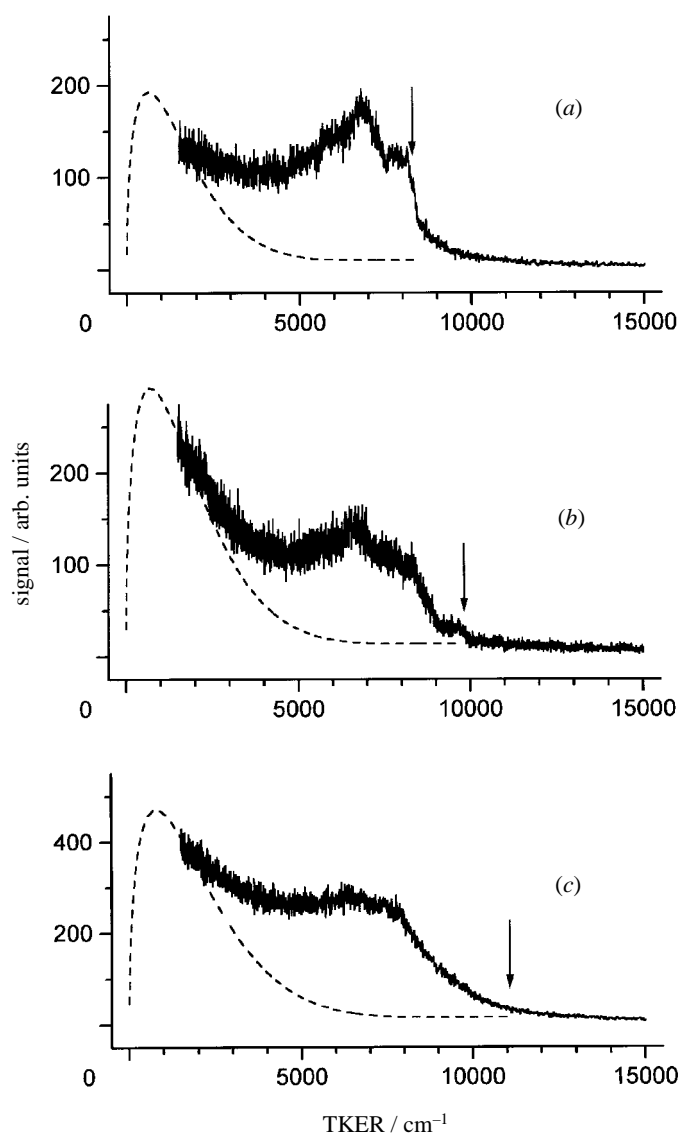


Figure 4. TKER spectra (derived assuming that the observed H atoms recoil from a partner fragment with mass 30 amu) obtained from CH_3NH_2 photolysis at (a) 233.3 nm (42854 cm^{-1}), (b) 225.4 nm (44357 cm^{-1}) and (c) 219.0 nm (45648 cm^{-1}) with, in each case, ε aligned at 90° to the TOF axis. The arrows indicate the maximum possible TKER assuming $D_0(\text{H-NHCH}_3) = 34550\text{ cm}^{-1}$. The dashed curves in (a) and (b) show the predicted form of the respective TKER spectra if a 'statistical' energy partitioning involving just NH bond fission is assumed.

endoergic for all excitation wavelengths used in this study. However, the N-H dissociation coordinate is seen to be very reminiscent of that in ammonia involving, first, a small potential barrier at short $R_{\text{N-H}}$ bond extensions and, at larger $R_{\text{N-H}}$, a CI with the ground-state surface at geometries for which the NH_2 moiety and one of the C-H bonds are coplanar. The calculations indicate a barrier height of *ca.* 3000 cm^{-1} and that electronically excited $\text{CH}_3\text{NH}(\tilde{A})$ fragments are only energetically allowed

for $\lambda < 210$ nm. If reliable, these values imply that even the energy provided by our longest photolysis wavelength (233.3 nm) is just sufficient that, if appropriately redistributed, \tilde{A} state CH_3NH_2 molecules are able to evolve over, rather than through, the potential barrier in the exit channel. They also indicate that, for the present experiments, ground-state CH_3NH fragments are the only thermodynamically allowed products that can result from the N–H bond fission process. We surmise that, as in ammonia, the effect of the \tilde{A}/\tilde{X} CI will be to channel any out-of-plane motion in the excited parent molecule into fragment internal (particularly rotational) excitation. Such an expectation is consistent with all of the experimental observations, namely: (i) the TKER spectra obtained at the longest excitation wavelength (figure 4a) indicates some formation of $\text{CH}_3\text{NH}(\tilde{X})$ fragments with no internal excitation, but the majority are formed with $E_{\text{int}} \gg 0$; (ii) the separations (*ca.* 900 cm^{-1}) of the ‘steps’ apparent in the TKER spectra recorded at the longer excitation wavelengths are consistent with that expected for the in-plane HNC bending vibration in the CH_3NH fragment (Dyke *et al.* 1989)—a mode which, on Franck–Condon grounds and by analogy with NH_3 photolysis, we would expect to be active during the dissociation process; and (iii) the proportion of internally ‘cold’ fragments declines as the excitation energy increases (see figure 4).

The TKER spectra shown in figure 4 and elsewhere (Reed *et al.* 1996) all appear bimodal, with a second maximum peaking at low kinetic energies. Our studies involving the various isotopomers of methylamine indicate that these slow H/D atoms also arise via dissociation channel (1.4). Such a result contradicts the suggestion of Waschewsky *et al.* (1995), who favoured channel (1.3) as the source of these slow H atoms, though, like these authors, we assume that these H atoms arise from unimolecular decay of highly vibrationally excited ground-state molecules (henceforth represented as $\text{CH}_3\text{NH}_2^\#$) formed by IC from the initially populated \tilde{A} state. The dashed curves in figures 4a, b illustrate the form of the TKER spectra that would be expected for the $\text{H} + \text{CH}_3\text{NH}$ products arising in the 233.3 and 225.4 nm photolysis of CH_3NH_2 if we assume (i) complete vibrational energy randomization in the $\text{CH}_3\text{NH}_2^\#$ molecules and (ii) that the probability of forming fragment pairs with any particular total kinetic energy, E_{kin} , is thus proportional to the total density of product states, ρ , at that energy. For simplicity, this $\rho(E)$ function is modelled as the product of just the CH_3NH fragment vibrational state density $N(E_v)$, at each energy E_v above the dissociation threshold, and a term $(E_{\text{kin}})^{1/2}$ (where $E_{\text{kin}} = E - E_v$) representing the three-dimensional translational density of states of the recoiling fragments (Reed *et al.* 1996). $N(E_v)$ is calculated using the Whitten–Rabinovitch approximation (Robinson *et al.* 1972) together with the harmonic normal mode frequencies listed in table 1. Rotational excitation is ignored in these calculations. The model calculations support the premise that the observed TKER spectra should be viewed in terms of a ‘direct’ or ‘dynamical’ component (associated with N–H bond extension on the \tilde{A} state surface and coupling via the CI to the $\text{H} + \text{CH}_3\text{NH}(\tilde{X})$ asymptote) and a ‘statistical’ component resulting from unimolecular decay of $\text{CH}_3\text{NH}_2^\#$ molecules. Further, they suggest that the two routes make comparable contributions to the total H atom yield following excitation at these wavelengths, though we concede that a more reliable estimate of this branching requires TKER spectra displaying a better signal to noise ratio and taken at more than one photolysis laser polarization to confirm the small angular anisotropy reported following photolysis at 222 nm (Waschewsky *et al.* 1995), and that β is insensitive to the product kinetic energy.

The finding that channel (1.4) provides the major contribution to the yield of

Table 1. Normal mode vibrational frequencies of CH_3NH_2 and the CH_3NH fragment used in the RRKM calculations described in this work

normal mode frequencies (cm^{-1})	
$\text{CH}_3\text{NH}_2^{\text{a}}$	3361, 2961, 2820, 1623, 1473, 1430, 1130, 1044, 780, 3427, 2985, 1485, 1455, 1195, 268
$\text{CH}_3\text{NH}^{\text{b}}$	3293, 2924, 2826, 1450, 1402, 1292, 1018, 964, 964, 2867, 1460, 966, 266

^aMotte-Tollet *et al.* (1992).

^bAll reduced by 10%, cf. the *ab initio* values reported by Dyke *et al.* (1989).

slow H atoms arising via the ‘statistical’ fragmentation pathway is significant. If we assume complete energy randomization in the $\text{CH}_3\text{NH}_2^{\#}$ molecules formed as a result of IC from the initially excited \tilde{A} state, then RRKM theory should provide a reasonable estimate of the energy dependent rate constant, $k(E)$, for unimolecular decay via the bond fissions (1.2)–(1.4). This can be estimated, for each dissociation path and for each excess energy ($E - D_0$), via the standard expression (Robinson *et al.* 1972)

$$k(E) = \sum_{E=D_0}^E P(E - D_0) \frac{1}{hN(E)}, \quad (3.2)$$

where the numerator represents the number of vibrational states in the respective transition states with energy $E > D_0$ and $N(E)$ is the vibrational state density of the parent CH_3NH_2 molecule at internal energy E . The respective sum of states terms for the transition states leading to C–N, C–H and N–H bond fission can be calculated using the Whitten–Rabinovitch approximation (Robinson *et al.* 1972), i.e.

$$\sum_{E_v=0}^{E_v} P(E_v) = \frac{(E_v + aE_z)^s}{s! \prod h\nu_i}, \quad (3.3)$$

where E_v is the fragment vibrational energy measured from the zero-point energy E_z (both calculated using the normal mode frequencies listed in table 1), a is parametrized as in Reed *et al.* (1996), the respective bond strengths are as listed in the Introduction and s ($= 14$) is the total number of vibrational modes bar the dissociation coordinate. We assume that twelve of the normal mode frequencies in each transition state retain their ground-state values (see table 1). For the transition state associated with N–H fission, the NH_2 asymmetric stretch ($\nu = 3427 \text{ cm}^{-1}$) becomes the reaction coordinate, whilst the wavenumbers of the NH_2 deformation and the NH_2 twist ($\nu = 1623$ and 1455 cm^{-1} , respectively) are both arbitrarily reduced to 200 cm^{-1} . The transition states associated with C–H and C–N bond fission are treated similarly. For C–H bond fission, the C–H asymmetric stretch vibration ($\nu = 2961 \text{ cm}^{-1}$) becomes the reaction coordinate and the wavenumbers of the CH_3 deformations (1485 and 1473 cm^{-1}) are reduced to 200 cm^{-1} ; for C–N bond fission, the C–N stretch ($\nu = 1044 \text{ cm}^{-1}$) disappears, the NH_2 twist ($\nu = 1455 \text{ cm}^{-1}$) is reduced to 200 cm^{-1} and the torsional frequency is lowered to 30 cm^{-1} . Figure 5 shows a plot of the unimolecular decay rate constants, $k(E)$, so derived, and of the energy dependence of the ratio $k_{\text{N-H}}/k_{\text{total}}$. Clearly, in the limit of complete energy

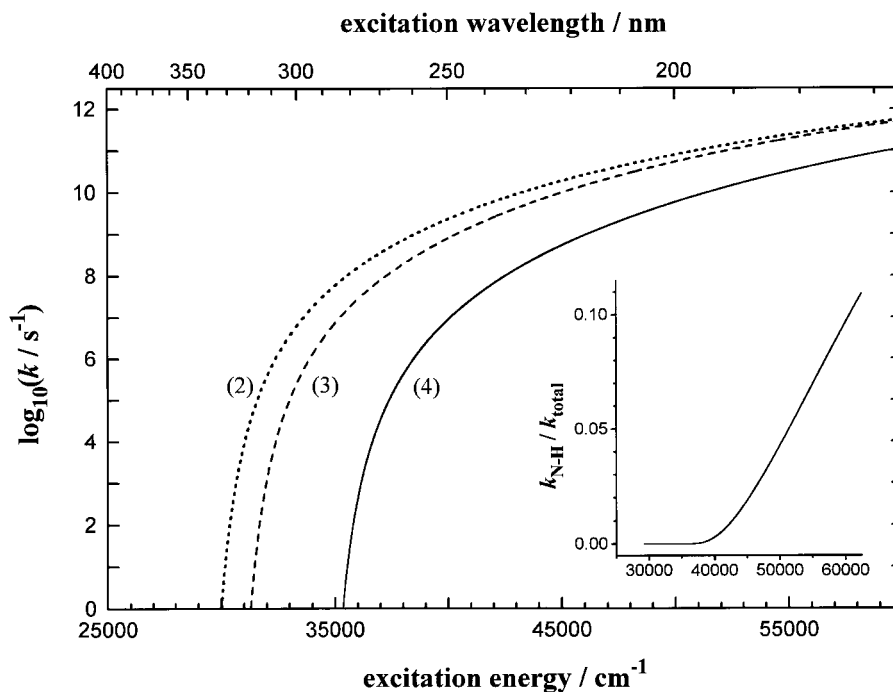


Figure 5. Calculated unimolecular decay rate constants, $k(E)$, for the C–N (1.2), C–H (1.3) and N–H (1.4) bond fission channels assuming complete energy randomization within the $\text{CH}_3\text{NH}_2^\#$ molecules before dissociation. The inset shows that under such circumstances N–H bond fission would make, at most, a minor contribution to the total dissociation yield at all UV excitation energies.

randomization within the $\text{CH}_3\text{NH}_2^\#$ molecules before dissociation, and irrespective of the precise frequencies we assume for the various transition state modes of vibration, RRKM theory predicts only a minor role for the N–H bond fission process.

Such a conclusion contradicts the experimental observations. The H atom kinetic energy distributions observed from photodissociation of CH_3NH_2 and CD_3NH_2 are very similar, whilst the D atom yield from the latter is small (Reed *et al.* 1996). Similar comments apply for the D atom kinetic energy distributions observed from CH_3ND_2 and CD_3ND_2 photolysis. The earlier quantum yield estimates (Michael *et al.* 1963) ascribed *ca.* 75% of the total dissociation to N–H bond fission. None of these results accord with the predictions arising from the RRKM modelling outlined above. Indeed, in the limit of complete energy randomization within the $\text{CH}_3\text{NH}_2^\#$ molecules before dissociation, we should expect C–N bond fission to make the greatest contribution to the dissociation products arising from these ‘hot’ ground-state molecules (see figure 5)—yet the quantum yield of channel (1.2) is less than 0.05 (Michael *et al.* 1963). Further, Waschewsky *et al.* (1995) show that the TKER spectrum of the small yield of $\text{CH}_3 + \text{ND}_2$ fragments resulting from 222.0 nm photolysis of CH_3ND_2 peaks away from zero, suggesting that they arise as a result of direct dissociation on the \tilde{A} state surface, and not from unimolecular decay of hot $\text{CH}_3\text{ND}_2^\#$ molecules. Thus, we conclude that the dissociation of these highly vibrationally excited $\text{CH}_3\text{NH}_2^\#$ molecules leads to a democratic sampling of that portion of the phase space associated with the $\text{H} + \text{CH}_3\text{NH}$ dissociation pathway, but not of the total available phase space. We take this to indicate that IC to the ground-state surface occurs

not in the vertical Franck–Condon region, but only after the occurrence of some (irreversible) N–H bond extension—most probably in the region of the conical section where we can expect the \tilde{A}/\tilde{X} coupling matrix elements to be largest. We may also speculate that the large mass ratio between C or N compared with H or D inhibits facile randomization between the —NH₂ and H₃CN— vibrational modes.

(c) *Ammonia photolysis: the ‘statistical’ channel*

Our earlier consideration of this channel (Mordaunt *et al.* 1996b) started with the premise that IC from the 0⁰ and 2¹ levels of \tilde{A} state ammonia molecules occurred in the inner well and thus constituted another population loss process (additional to tunnelling) which could contribute to the measured (lifetime limited) parent absorption linewidths. However, given the foregoing interpretation of the methylamine TKER spectra, involving IC in the outer well associated with the \tilde{A}/\tilde{X} CI, it is worth considering whether a similar model could explain the ‘statistical’ contribution to the H/D atom TOF spectra resulting from photolysis of the various isotopomers of ammonia. The measured total population loss rates (Henck *et al.* 1995) from both the 0⁰ and 2¹ levels increase in the order ND₃ < ND₂H < NDH₂ < NH₃, consistent with H(D) atom loss via a tunnelling mechanism. So, too, is the observation that the H/D product ratio from dissociation of the mixed isotopomers is always much greater than unity (Mordaunt *et al.* 1996b). For each isotopomer, population in the 0⁰ level decays faster than from the corresponding 2¹ level. This reflects the fact that the exit channel barrier is smallest, and tunnelling consequently most facile, at planar geometries: the wavefunction for the 2¹ level has a node at planarity, so molecules in this level have to penetrate a larger effective barrier in order to dissociate (Ashfold *et al.* 1985).

IC rates will depend on the background density of states and the strength of the matrix elements coupling the \tilde{A} and \tilde{X} states. The vibrational state densities of NH₃(\tilde{X}) and ND₃(\tilde{A}) at the energy of the state origin are, respectively, *ca.* 40 cm⁻¹ and 200 cm⁻¹ (in the harmonic approximation). However, nuclear permutation symmetry must be conserved during the IC process and, as a result, for any given \tilde{A} state level, the effective background state density for both NH₃ and ND₃ is reduced six fold (Mordaunt *et al.* 1996b). NH₂D and NHD₂ have lower symmetry; in this case, permutation symmetry requirements only introduce a two-fold reduction in the total background vibrational state density (*ca.* 100 cm⁻¹). Clearly, density of states arguments alone cannot account for the isotopic dependence of the \tilde{A} state population loss rates but the larger ‘effective’ density of receptor states in the case of NH₂D and NHD₂ is consistent with the larger ‘statistical’ contribution to the TKER spectra obtained when photolysing these molecules (see figures 1 and 2). Progressing this argument further is difficult without some knowledge of the way the $\tilde{A} \rightarrow \tilde{X}$ coupling matrix elements vary with isotopic substitution, but the balance of evidence must favour tunnelling through the barrier in the N–H(D) exit channel as the dominant population loss mechanism from the inner well of the \tilde{A} state potential energy surface.

Thus, by analogy with methylamine, we now consider a model where the process we have termed IC, leading to a ‘statistical’ product energy disposal, occurs in the region of the \tilde{A}/\tilde{X} conical intersection. Specifically, we propose that outgoing trajectories which pass through the CI on the first encounter evolve without impediment towards the H + NH₂(\tilde{X}) asymptote, i.e. after tunnelling through the exit channel barrier, these dissociations are essentially ‘direct’. The topology of the parent \tilde{A} and \tilde{X} state

potential energy surfaces along the N–H dissociation coordinate dictates the form of the excess energy disposal associated with this ‘dynamical’ fragmentation pathway (substantial *a*-axis rotation of the fragment) and the product state dependent μ – ν correlations (Dixon 1996; Mordaunt *et al.* 1996*a,b*). The magnitudes of the β parameters determined for the extremes of maximum and minimum product rotation are also consistent with direct passage through the CI since, as discussed below, molecules which survive in this outer well for several vibrational periods are unlikely to yield particularly anisotropic product recoil distributions.

Now consider that fraction of the outgoing trajectories that fail to pass through the CI on the first pass. The systems studied in this work all have insufficient energy to reach the H + NH₂(\tilde{A}) asymptote and thus must be reflected back towards shorter R_{N–H} bond lengths. Clearly, if the associated trajectories pass through the CI during this compressive stage, momentum conservation dictates that they will be drawn into the deep \tilde{X} state well. Here they can explore much of the available phase space and substantial intramolecular vibrational redistribution (IVR) is to be expected. This, we propose, is the mechanism, hitherto termed IC, which leads to the underlying ‘statistical’ component in the experimentally observed TKER spectra. As discussed previously, one key requirement for $\tilde{A} \rightarrow \tilde{X}$ transfer is planarity. Thus it is pertinent to note that, of all the fragmentations studied, it is the dissociation of ND₃ molecules following excitation to their 0⁰ level that yields the highest ratio of ‘dynamical’ to ‘statistical’ fragment energy disposal. It is this isotopomer that, in its zero point level, has the smallest out-of-plane vibrational amplitude and for which the barrier tunnelling process will provide the greatest discrimination in favour of planar dissociations and thus passage through the CI on the first (extensive) encounter.

At the opposite extreme, consider the TKER spectrum for the D + NHD products arising from the dissociation of NHD₂ molecules following excitation to their 2¹ level (figure 3). The present model assumes that all of these fragmentations start by tunnelling out of the inner well; thus the bulk of the NHD₂ molecules will start to dissociate by extending R_{N–H} rather than R_{N–D}. Of the former, those that pass directly through the CI will yield H + ND₂ products, with a dynamical energy disposal (figure 2*b*). However, any reflected trajectories which traverse the CI whilst R_{N–H} is contracting will, again, have the chance to explore large portions of the \tilde{X} state surface and redistribute the vibrational energy initially concentrated in the N–H bond amongst all of the available degrees of freedom. Density of state considerations suggest that the ultimate decomposition of these ‘hot’ ground-state molecules will yield either an H or D atom, with relative probabilities of *ca.* 1:2 (Mordaunt *et al.* 1996*b*). Both of these pathways should exhibit ‘statistical’ TKER spectra. Hence the continuum underlying the structured ‘dynamical’ contribution to the H + ND₂ product yield spectrum (figure 2*e*) and, most tellingly, the observation (figure 3) that the TKER spectrum of the D + NHD products is almost entirely ‘statistical’; the very small structured contribution superimposed on this continuum is attributable to the small fraction of parent molecules that dissociate by D atom tunnelling and direct passage through the conical intersection in the R_{N–D} dissociation coordinate.

4. Conclusion

The bimodality of the TKER spectra derived from TOF measurements of the H/D atoms resulting from near UV photolysis of methylamine and various of its isotopomers is consistent with there being both ‘dynamical’ (higher kinetic energy) and

'statistical' (slower) contributions to the total H+CH₄N dissociation yield. N–H bond fission is shown to be responsible for the bulk, if not all, of the H atom yield. Both contributions are considered to arise as a result of one H atom tunnelling through (or passing over) an earlier barrier in the N–H dissociation coordinate and evolving into the region of the conical intersection between the \tilde{A} and \tilde{X} state surfaces. 'Dynamical' energy disposal is associated with those molecules which pass directly through this CI and evolve out to the ground-state (H + CH₃NH(\tilde{X})) asymptote, whereas the 'statistical' contribution is attributed to those molecules that 'miss' the CI on the first encounter, but make the $\tilde{A} \rightarrow \tilde{X}$ transfer on a later encounter. This allows time for possible IVR on both the \tilde{A} and \tilde{X} state surfaces before dissociation and an apparently 'statistical' energy disposal.

Such an interpretation has triggered further consideration of the form of the TKER spectra derived from TOF measurements of the H/D atom products arising in the dissociation of various isotopomers of ammonia following excitation to the 0⁰ and 2¹ levels of their respective \tilde{A} states (Mordaunt *et al.* 1996*a, b*). A similar model which associates 'dynamical' energy disposal with those molecules that pass through the \tilde{A}/\tilde{X} CI during bond extension and 'statistical' kinetic energy release with those that transfer during NH(D) bond compression appears to provide a qualitative explanation for the way the observed H and/or D atom yields and their associated TKER spectra vary with excitation wavelength (0⁰ versus 2¹ band excitation) and isotopic composition.

We are grateful to the EPSRC and NERC for their support of this research, to colleagues in Universität Bielefeld, Germany (Professor K. H. Welge and Dr L. Schnieder) and in Bristol (Dr A. J. Orr-Ewing, Dr S. H. S. Wilson, Dr C. M. Western and Dr K. N. Rosser) for their many varied and important contributions to this programme and to Professor K. Lehmann (Princeton) for helpful correspondence. M.K. thanks the Japanese Society for the Promotion of Science for the award of a Postdoctoral Research Fellowship.

References

- Ashfold, M. N. R., Bennett, C. L. & Dixon, R. N. 1985 *Chem. Phys.* **93**, 293–306.
Ashfold, M. N. R., Bennett, C. L. & Dixon, R. N. 1986 *Faraday Disc. Chem. Soc.* **82**, 163–175.
Ashfold, M. N. R., Dixon, R. N., Irving, S. J., Koeppe, H.-M., Meier, W., Nightingale, J. R., Schnieder, L. & Welge, K. H. 1990 *Phil. Trans. R. Soc. Lond. A* **332**, 375–386.
Ashfold, M. N. R., Mordaunt, D. H. & Wilson, S. H. S. 1996 In *Advances in photochemistry* (ed. D. C. Neckers, D. H. Volman & G. von Bünau), vol. 21, pp. 217–295 (and references therein). New York: Wiley.
Ball, S. M., Hancock, G. & Winterbotton F. 1995 *Faraday Disc. Chem. Soc.* **100**, 215–227.
Biesner, J., Schnieder, L., Schmeer, J., Ahlers, G., Xie, X., Welge, K. H., Ashfold, M. N. R. & Dixon, R. N. 1988 *J. Chem. Phys.* **88**, 3607–3616.
Biesner, J., Schnieder, L., Ahlers, G., Xie, X., Welge, K. H., Ashfold, M. N. R. & Dixon, R. N. 1989 *J. Chem. Phys.* **91**, 2901–2911.
Dixon, R. N. 1996 *Mol. Phys.* **88**, 949–977.
Douglas, A. E. 1963 *Faraday Disc. Chem. Soc.* **35**, 158–174.
Dunn, K. M. & Morokuma, K. 1996 *J. Phys. Chem.* **100**, 123–129.
Dyke, J. M., Lee, E. P. F. & Zamanpour Niavaran, M. H. 1989 *Int. J. Mass Spectrom. Ion Processes* **94**, 221–235.
Henck, S. A., Mason, M. A., Yan, W.-B., Lehmann, K. K. & Coy, S. L. 1995 *J. Chem. Phys.* **102**, 4772–4782, 4783–4792.
Hwang, S. M., Higashihara, T., Shin, K. S. & Gardiner Jr, W. C. 1990 *J. Phys. Chem.* **94**, 2883–2889.

- Kassab, E., Cleghorn, J. T. & Evleth, E. M. 1983 *J. Am. Chem. Soc.* **105**, 1746–1753.
- Lara, L. M., Lorenz, R. D. & Rodrigo, R. 1994 *Planet. Space Sci.* **42**, 5–14.
- Mack, J. A., Mikulecky, K. & Wodtke, A. M. 1996 *J. Chem. Phys.* **105**, 4105–4116 (and references therein).
- McCarthy, M. I., Rosmus, P., Werner, H.-J., Botschwina, P. & Vaida, V. 1987 *J. Chem. Phys.* **86**, 6693–6700.
- Michael, J. V. & Noyes, W. A. 1963 *J. Am. Chem. Soc.* **85**, 1228–1233.
- Miller, R. L., Suits, A. G., Houston, P. L., Toumi, R., Mack, J. A. & Wodtke, A. M. 1994 *Science* **268**, 1831–1838.
- Mordaunt, D. H., Lambert, I. R., Morley, G. P., Ashfold, M. N. R., Dixon, R. N., Western, C. M., Schnieder, L. & Welge, K. H. 1993 *J. Chem. Phys.* **98**, 2054–2065.
- Mordaunt, D. H., Ashfold, M. N. R. & Dixon, R. N. 1996a *J. Chem. Phys.* **104**, 6460–6471.
- Mordaunt, D. H., Dixon, R. N. & Ashfold, M. N. R. 1996b *J. Chem. Phys.* **104**, 6472–6481.
- Morley, G. P., Lambert, I. R., Ashfold, M. N. R., Rosser, K. N. & Western, C. M. 1992 *J. Chem. Phys.* **97**, 3157–3165.
- Morley, G. P., Lambert, I. R., Mordaunt, D. H., Wilson, S. H. S., Ashfold, M. N. R., Dixon, R. N. & Western, C. M. 1993 *J. Chem. Soc. Faraday Trans.* **89**, 3865–3875.
- Motte-Tollet, F., Hubin-Franskin, M.-J. & Collin, J. E. 1992 *J. Chem. Phys.* **97**, 7314–7322.
- Reed, C. L., Kono, M. & Ashfold, M. N. R. 1996 *J. Chem. Soc. Faraday Trans.* **92**, 4897–4904.
- Robinson, P. J. & Holbrook, K. A. 1972 *Unimolecular reactions*. New York: Wiley-Interscience.
- Rosmus, P., Botschwina, P., Werner, H.-J., Vaida, V., Engelking, P. C. & McCarthy, M. I. 1987 *J. Chem. Phys.* **86**, 6677–6692.
- Runau, R., Peyerimhoff, S. D. & Buenker, R. J. 1977 *J. Mol. Spectrosc.* **68**, 253–268.
- Takahashi, K., Kishigama, M., Matsumi, Y., Kawasaki, M. & Orr-Ewing, A. J. 1996 *J. Chem. Phys.* **105**, 5290–5293 (and references therein).
- Taylor, D. P. & Bernstein, E. R. 1995 *J. Chem. Phys.* **103**, 10453–10464.
- Tsuboi, M., Hirakawa, A. Y. & Kawashima, H. 1969 *J. Mol. Spectrosc.* **29**, 216–229.
- Vaida, V., Hess, W. & Roebber, J. L. 1984 *J. Phys. Chem.* **88**, 3397–3400.
- Waschewsky, G. C. G., Kitchen, D. C., Browning, P. W. & Butler, L. J. 1995 *J. Phys. Chem.* **99**, 2635–2645.

Discussion

M. J. J. VRAKING (*Department of Chemistry, Amsterdam University, The Netherlands*). Professor Ashfold presented beautiful results applying the hydrogen atom Rydberg time-of-flight technique introduced by Professor Karl Welge to studies of molecular photodissociation. Could he give us his opinion concerning the prospects for this technique in experiments with atoms other than hydrogen, or even small molecules?

M. N. R. ASHFOLD. Several factors contribute to the exquisite resolution and sensitivity of the H(D) atom photofragment translational spectroscopy (PTS) technique (Ashfold *et al.* 1996). The relevant $n = 2 \leftarrow n = 1$ and high $n \leftarrow n = 2$ transition cross sections in atomic H(D) are particularly large, so H(D) Rydberg atoms can be prepared with high efficiency using relatively modest laser powers, thereby minimizing any unintentional (and undesirable) competing multiphoton ionization processes. The lightness of the H(D) fragment offers a second unique advantage, which will persist even if it eventually proves possible to prepare suitable long-lived high- n Rydberg states of other heavier atoms or molecules with adequate efficiency. The H(D) atom probe laser is set at the centre of the $n = 2 \leftarrow n = 1$ Doppler profile

and we detect H(D) atoms that recoil at right angles to the parent beam direction. The recoil velocity, $\mathbf{v}_{\text{recoil}}$, of all but the very slowest H(D) atomic fragments is so much greater than the parent beam velocity, $\mathbf{v}_{\text{parent}}$, that the H(D) atom TOF spectrum recorded in the *laboratory* frame is essentially that which would be recorded if it was possible to perform the experiment in the *centre of mass* (CM) frame. No frame transformation is necessary, therefore, and the ultimate TKER spectrum has the full energy resolution of the original data. It is worth emphasizing that comparable photofragment kinetic energy resolution can also be obtained in suitably designed experiments in the limit that $\mathbf{v}_{\text{parent}} \gg \mathbf{v}_{\text{recoil}}$, as in the fast ion beam studies of, for example, Neumark and colleagues (1996). In the more usual situation involving relatively heavy fragments and $\mathbf{v}_{\text{recoil}} \sim \mathbf{v}_{\text{parent}}$, it is necessary to make measurements at several laboratory scattering angles and iterate a (inevitably cruder) trial CM recoil distribution until it can account for all the observed laboratory frame data. Thus, whilst many exciting possibilities can be envisaged as Rydberg (or metastable (Morgan *et al.* 1996)) tagging schemes are gradually extended to a wider range of atomic and molecular species it is not expected that such methods will provide fragment TKER spectra with the resolution or sensitivity achieved with the H(D) PTS technique.

R. N. DIXON. Dr Vrakking asked whether the proposed distinction between dynamic and statistical routes to the dissociation of ammonia and its isotopomers might be confirmed by time domain measurements, and would like to know the likely timescales. I have made a time-dependent quantum mechanical study of these processes for NH_3 (Dixon 1996) using the best available potential energy surfaces for the \tilde{A} and \tilde{X} states. These surfaces were restricted to C_s geometry, with three active vibrational coordinates (one NH bondlength, the deformation of the opposite HNH angle, and the out-of-plane coordinate). The remaining vibrational coordinates (two NH bondlengths and an in-plane angle) were frozen at their equilibrium values. The timescale of the dynamical channel should be little affected by this restriction, but the lifetime of statistical decay via the ground state surface is probably underestimated by these calculations.

The dissociation via the first two vibronic levels of the excited state is controlled by tunnelling through the small barriers in each exit channel, and the rate is very sensitive to the assumed barrier height. The calculations predict lifetimes of *ca.* 1 ps (which is considerably longer than an estimate of *ca.* 200 fs from observed linewidths), with little apparent delay between the direct and statistical components of the NH_2 population distribution. An RRKM estimate of the lifetime for $\text{NH}_3^{\ddagger} \rightarrow \text{H} + \text{NH}_2$ at the available energy of 9000 cm^{-1} is rather less than 1 ps. These rates will be isotope dependent. Even so, the calculations suggest that tunnelling will be the rate-determining step. Thus it is doubtful that there will be any clear distinction between the rates of decay through the dynamical and statistical channels, although the statistical decay may be delayed up to 1 ps.

I. M. MILLS (*Department of Chemistry, University of Reading, UK*). I know that vibrational density-of-states functions are difficult to calculate accurately for an anharmonic potential energy surface for energies approaching dissociation. Can Professor Ashfold comment on whether this was a significant problem in his work, and describe how he did this calculation?

M. N. R. ASHFOLD. For different reasons this was not a significant problem in modelling either NH_3 or CH_3NH_2 fragmentation. The D + NHD product state density

shown in figure 3 was based on the harmonic oscillator, rigid rotor approximation in which each vibration was treated individually whereas the rotational and translational contributions to the total state density were treated semi-classically. The energy range involved lies well below any dissociation limit of the NHD fragment, thus neglect of anharmonicity is unlikely to introduce significant error in this calculation. Rather, we expect neglect of centrifugal distortion effects to be the greatest omission in this calculation, resulting in an underestimate of the total product state density at low TKER.

The calculated unimolecular decay rates of CH_3NH_2 via C–N, C–H and N–H bond fission (figure 5) require estimation of the total density of states associated with the various transition states. Obviously, considerable uncertainties attach to (at least some of) the frequencies associated with the various transition states. Even so, as discussed in our paper, the use of the Whitten–Rabinovitch approximation and the neglect of the rotational degrees of freedom are unlikely to invalidate the overall conclusion that N–H bond fission should be, at best, a minor fragmentation channel for CH_3NH_2 molecules in which the internal excitation is truly randomly distributed.

Additional references

- Butler, L. J. & Neumark, D. M. 1996 *J. Phys. Chem.* **100**, 12 801–12 816 (and references therein).
Morgan, C. G., Drabbels, M. & Wodtke, A. M. 1996 *J. Chem. Phys.* **105**, 4550–4555 (and references therein).